

Spectral Identification of Buried Unexploded Ordnance from Low-Frequency Electromagnetic Data

Stephen J. Norton and I. J. Won

Geophex, Ltd., 605 Mercury Street, Raleigh, NC 27603

Ernesto R. Cespedes

US Army Engineer Research and Development Center,
3909 Halls Ferry Road, Vicksburg, MS 39180

Received January 30, 2001; revised April 17, 2001

A procedure is described for identifying buried unexploded ordnance (UXO) from their spectral signatures derived from electromagnetic induction (EMI) data. Using the dipole response of the UXO as a first approximation, it can be shown that data obtained from a target at an arbitrary depth and orientation can be expressed as a linear combination of the target's longitudinal and transverse responses. The latter are pre-measured for a set of UXO and stored in a spectra library. The measured spectrum from an unknown target can then be compared to the library spectra to identify the UXO type. The optimal linear combination of the longitudinal and transverse responses that produce the best fit to the measured spectra is obtained by a maximum likelihood procedure. The method is demonstrated using data derived from UXO and sections of metallic pipe of different sizes, shapes and material.

Key Words. Unexploded ordnance, electromagnetic induction, subsurface detection, target identification, target recognition.

1. Introduction

Magnetometry and electromagnetic induction (EMI) sensors have been shown to be effective tools for detecting buried unexploded ordnance (UXO), but the task of identifying the type of UXO or of discriminating between UXO and metallic debris (clutter) has proved to be much more challenging. If only a fraction of detected anomalies could be identified as

clutter, significant savings in excavation costs would result. We describe a new methodology for the discrimination and identification of UXO based on their multi-frequency EMI response.

Geophex, Ltd., has developed a series of broadband electromagnetic induction sensors [1–3] for detecting buried conducting anomalies. These sensors have also recently been shown to be effective in identifying buried UXO. The Geophex GEM-3 sensor, which uses co-axial transmit and receive coils, is particularly well suited for this purpose because of its multi-frequency capability and its compact spatial footprint [2]. This instrument also employs a unique transmit-bucking scheme to null the primary field at the location of the receiving coil. The GEM-3 typically operates over a range of frequencies from 30 Hz to about 24 kHz.

Each UXO type generates a characteristic spectral response which is a function of its size, shape and composition (conductivity and permeability). A reasonable methodology for identifying UXO is to record first a set of "library spectra" derived from a set of known UXO types. Identification of an unknown target can then be performed by comparing spectral data acquired from the target to the set of library spectra. Unfortunately, a direct comparison between the raw sensor data and the library data is usually not feasible because the UXO spectrum (both its shape and magnitude) varies with the object's orientation and distance from the sensor head. Consequently, additional signal processing needs to be performed to remove this dependence on range and orientation.

One approach is to attempt to estimate the target orientation directly by fitting EMI data to a dipole model [4–7]. One version of this method performs a nonlinear search for seven parameters that characterize the target: the x , y and z coordinates of its centroid, two angles defining its orientation, and two eigenvalues characterizing its longitudinal and transverse responses. A related approach, which does not require a parameter search over orientation, attempts to measure directly the matrix elements of the magnetic polarizability tensor [7]. This tensor is a 3 by 3 matrix, defined below in Eq. (1), that characterizes the target response and represents the first term in a multipole expansion of the scattered field. The matrix is then diagonalized; its eigenvalues are orientation invariant and are used as the spectral signatures to be compared to the UXO library spectra. The above two approaches are, however, relatively labor intensive since they require EMI data acquired at multiple points above the target. These methods are also fairly sensitive to uncertainties in the positions of the measurements relative to the target.

In this paper we describe a procedure that does not require accurate knowledge of the relative sensor/target position, provided only that the

sensor/target separation is small enough to provide an adequate target signal. We shall assume here that the targets of interest are axially symmetric which, to a reasonable approximation (e.g., ignoring fins), is true of almost all UXO. In the far field, defined as sufficiently far away so that the lowest-order term in the multipole expansion dominates (the dipole term), the EMI response of an axially-symmetric target is entirely characterized by its longitudinal and transverse spectral responses [8]. This dipole approximation is quite good when the target/sensor separation is at least three or four times the target size. The longitudinal and transverse responses correspond, respectively, to incident fields parallel and perpendicular to the target axis. By "incident fields," we mean the field generated by the transmit coil at the target and the (hypothetical) field generated by the receiver coil if it were used as a transmitter. Both of these fields are incident from the same direction in the case of the monostatic GEM-3 sensor.

For a UXO at an arbitrary orientation, the recorded spectrum can be expressed as a linear combination of its longitudinal and transverse responses. Our procedure is to determine the linear combination that provides the best fit to the measured response. This methodology is presented in the next section. The technique is then demonstrated in Section 3 on a set of metallic pipes of different sizes and compositions, and in Section 4, on eleven different UXO.

2. Matching UXO Data to Library Signatures

From reciprocity principles, the response of the sensor can be expressed in the following general form [8-10]

$$V(\omega) = \mathbf{H}_T \cdot \mathbf{P}(\omega) \cdot \mathbf{H}_R \quad (1)$$

where $V(\omega)$ is the emf induced in the receiving coil. Here \mathbf{H}_T is the incident magnetic field at the location of the target (i.e., the field in the absence of the target) generated by the transmitting coil. Similarly, \mathbf{H}_R is the incident field generated by the receiving coil if it were used as a transmitter. In Eq. (1), the target is characterized by $\mathbf{P}(\omega)$, which is a 3 by 3 complex, symmetric matrix known as the magnetic polarizability tensor. Equation (1) can be identified as the first term (the dipole term) in a multipole expansion of the target response in which the higher order terms have been neglected.

If the skin depth in the earth in which the target is embedded is long compared to the target depth, then the fields \mathbf{H}_T and \mathbf{H}_R may be regarded as frequency independent and the frequency response of the target is contained in the tensor $\mathbf{P}(\omega)$ only. This approximation is valid for real earth conductivities (under 1 S/m), typical EMI frequencies (under 100 kHz), and typical UXO depths (0 to 2 m).

For an axial-symmetric target, one can write

$$\mathbf{P}(\omega) = \mathbf{O}\Lambda(\omega)\mathbf{O}^T \quad (2)$$

where \mathbf{O} is a rotation matrix, and

$$\Lambda(\omega) = \begin{pmatrix} \beta_L(\omega) & 0 & 0 \\ 0 & \beta_T(\omega) & 0 \\ 0 & 0 & \beta_T(\omega) \end{pmatrix} \quad (3)$$

The complex eigenvalues $\beta_L(\omega)$ and $\beta_T(\omega)$ characterize, respectively, the longitudinal and transverse responses of the target. These are independent of target orientation, and thus serve as our intrinsic target signatures when measured over a range of frequencies.

When Eqs. (3) and (2) are substituted into (1) and the matrices multiplied out, the result is a linear combination of the two eigenvalues:

$$V(\omega) = s_L \beta_L(\omega) + s_T \beta_T(\omega) \quad (4)$$

where the coefficients s_L and s_T depend on the incident fields and their angles of incidence, but are assumed independent of frequency. For example, if a monostatic sensor is positioned directly over the target and the axis of the target is inclined by an angle θ from the vertical, one can show that $s_L = A \cos^2 \theta$ and $s_T = A \sin^2 \theta$, where A is an amplitude factor depending on the incident field strengths and the target/sensor separation.

Our approach is to measure the longitudinal and transverse responses of a set of known targets by placing the sensor over each target and recording its response while the target is in the vertical and horizontal orientations relative to the sensor axis; this yields $\beta_L(\omega)$ and $\beta_T(\omega)$, respectively. The measurement is performed at M discrete frequencies, ω_k , $k = 1, \dots, M$. The resulting $\beta_L(\omega_k)$ and $\beta_T(\omega_k)$ are then stored in a UXO "library" or data base. Then, given a set of multi-frequency measurements, $V(\omega_k)$, over an unknown target, we compute the mean-square error

$$E = \sum_{k=1}^M w_k |V(\omega_k) - s_L \beta_L(\omega_k) - s_T \beta_T(\omega_k)|^2 \quad (5)$$

for each set of library spectra $\beta_L(\omega)$ and $\beta_T(\omega)$ in turn. In Eq. (5), w_k is a positive weighting factor that may account, if desired, for differences in the signal-to-noise ratio of the data. The library spectrum that produces the smallest mean-square error, E , is then used to identify the most likely target. The coefficients s_L and s_T are computed for every library spectrum by selecting the coefficients that minimize E for that spectrum. This is done by setting $\partial E / \partial s_L = 0$ and $\partial E / \partial s_T = 0$, which leads to two linear equations in the two unknowns s_L and s_T . The solution to this system is

$$s_L = (A_{22}b_1 - A_{12}b_2)/D \quad (6a)$$

$$s_T = (-A_{12}b_1 + A_{11}b_2)/D \quad (6b)$$

$$D = A_{11}A_{22} - A_{12}^2 \quad (6c)$$

where

$$A_{11} = \sum_{k=1}^M w_k |\beta_L(\omega_k)|^2 \quad (7a)$$

$$A_{22} = \sum_{k=1}^M w_k |\beta_T(\omega_k)|^2 \quad (7b)$$

$$A_{12} = \text{Re} \sum_{k=1}^M w_k \beta_L(\omega_k) \beta_T(\omega_k)^* \quad (7c)$$

$$b_1 = \text{Re} \sum_{k=1}^M w_k V(\omega_k) \beta_L(\omega_k)^* \quad (7d)$$

$$b_2 = \text{Re} \sum_{k=1}^M w_k V(\omega_k) \beta_T(\omega_k)^* \quad (7e)$$

We remark that, under the assumption of a Gaussian noise model, the weights s_L and s_T obtained in this way are the maximum-likelihood values of these parameters. Note that for a solution to exist, the determinant D given by Eq. (6c) must not vanish; this will hold whenever

$$\left[\text{Re} \sum_{k=1}^M w_k \beta_L(\omega_k) \beta_T(\omega_k)^* \right]^2 < \sum_{k=1}^M w_k |\beta_L(\omega_k)|^2 \sum_{k=1}^M w_k |\beta_T(\omega_k)|^2 \quad (8)$$

Equality will result whenever $\beta_L(\omega_k) = c\beta_T(\omega_k)$, where c is a constant independent of frequency. This is the case for a sphere, for which $\beta_L(\omega_k) = \beta_T(\omega_k) = \beta(\omega_k)$. In this situation, Eq. (5) can be replaced by

$$E = \sum_{k=1}^M w_k |V(\omega_k) - s\beta(\omega_k)|^2 \quad (9)$$

and the s that minimizes E is

$$s = \frac{\text{Re} \sum_{k=1}^M w_k V(\omega_k) \beta(\omega_k)^*}{\sum_{k=1}^M w_k |\beta(\omega_k)|^2} \quad (10)$$

Recall that the β s will be pre-measured and stored in a spectra library. For objects that are non-spherical (or have some reasonable aspect ratio), the condition (8) will hold and two weights will be computed. For spherical-like objects in the library, we employ one β and a single weight, which is given by Eq. (10).

For a conducting target, the output of the sensor is a complex quantity with its real and imaginary parts identified with the inphase and quadrature components of the recorded signal. In the above analysis, s_L weights both the inphase and quadrature components of the longitudinal response and, similarly, s_T weights both components of the transverse response. This is a consequence of Eq. (4), which follows from the model (1) and the assumption that the fields H_T and H_R are real. The latter assumption will hold when the skin depths in the earth are long compared to the target depth. However, a somewhat more general approach is to consider a linear combination of the inphase and quadrature components separately. In other words, we write

$$V(\omega) = s_L^{(I)} \beta_L^{(I)}(\omega) + s_T^{(I)} \beta_T^{(I)}(\omega) + i[s_L^{(Q)} \beta_L^{(Q)}(\omega) + s_T^{(Q)} \beta_T^{(Q)}(\omega)] \quad (11)$$

instead of Eq. (4), where the β s have now been separated into their real and imaginary parts by writing $\beta_L = \beta_L^{(I)} + i\beta_L^{(Q)}$, and $\beta_T = \beta_T^{(I)} + i\beta_T^{(Q)}$. We now wish to minimize

$$E = \sum_{k=1}^M w_k |V(\omega_k) - s_L^{(I)} \beta_L^{(I)}(\omega_k) - s_T^{(I)} \beta_T^{(I)}(\omega_k) - i[s_L^{(Q)} \beta_L^{(Q)}(\omega_k) + s_T^{(Q)} \beta_T^{(Q)}(\omega_k)]|^2 \quad (12)$$

with respect to the four weights $s_L^{(I)}$, $s_T^{(I)}$, $s_L^{(Q)}$ and $s_T^{(Q)}$. This leads to a set of equations for the weights similar to (6), but now all quantities are real. This approach, where we fit the data using four independent weights instead of two, resulted in fewer identification errors for our data sets. For data acquired on a test stand, best results (fewest errors) were obtained using all four weights. However, for data acquired over buried targets, best results were obtained using only the quadrature component of the data. That is, for the latter case, we discarded the inphase part of the signal and compared only the quadrature component of $V(\omega_k)$ to $\beta_L^{(Q)}(\omega_k)$ and $\beta_T^{(Q)}(\omega_k)$. This gave better results because the quadrature component is generally less sensitive to background variations in the soil.

3. Measurement and Identification of Test Site Targets

Twenty one targets, listed in Table 1, are buried in a test site on Geophex's property. The targets are lengths of pipe of different sizes and compositions. There are nine distinct target types identified by the letters A through I. The subscript attached to the letter in Table 1 indicates that a target of a particular type was buried in several different locations, typically at different orientations and/or depths. The depths are measured from the surface to the centroid of the target. Before data were taken at the test site,

Table 1. Targets (Lengths of Metallic Pipe) Buried at the Geophex Test Site

ID	Length (in)	OD (in)	Weight (lb)	Composition	Orientation	Depth (in)
A ₁	20	6.1	30.0	Steel	Horizontal	40
A ₂	20	6.1	30.0	Steel	45 Degrees	44
B ₁	18	3.1	11.0	Steel	Vertical	28
B ₂	18	3.1	11.0	Steel	45 Degrees	32
B ₃	18	3.1	11.0	Steel	Horizontal	28
C ₁	12	2.5	6.0	Steel	Horizontal	20
C ₂	12	2.5	6.0	Steel	45 Degrees	24
C ₃	12	2.5	6.0	Steel	Horizontal	24
D	12	2.5	2.0	Aluminum	Horizontal	20
E ₁	6	1.6	1.38	Steel	Vertical	12
E ₂	6	1.6	1.38	Steel	45 Degrees	12
E ₃	6	1.6	1.38	Steel	Horizontal	12
E ₄	6	1.6	1.38	Steel	45 Degrees	8
F ₁	4	1.6	0.91	Steel	Horizontal	12
F ₂	4	1.6	0.91	Steel	Horizontal	12
G ₁	6	0.9	0.09	Aluminum	Horizontal	6
G ₂	6	0.9	0.09	Aluminum	Horizontal	6
H ₁	6	0.9	0.25	Copper	45 Degrees	8
H ₂	6	0.9	0.25	Copper	Horizontal	6
I ₁	4	0.8	0.38	Steel	Horizontal	4
I ₂	4	0.8	0.38	Steel	Horizontal	4

identical copies of the nine target types were placed on a test stand and spectra recorded both in the vertical and horizontal orientations to obtain the longitudinal and transverse response functions $\beta_L(\omega)$ and $\beta_T(\omega)$. Ten discrete frequencies were used in the measurements at 30, 90, 150, 270, 570, 1230, 2610, 5430, 11430, 20070 Hz.

Data were then recorded over the 21 buried targets in the test site. Using the GEM-3 sensor, the earth at the site was found to have an apparent conductivity of approximately 0.05 S/m and an apparent relative magnetic susceptibility of approximately 2×10^{-4} . Five measurements were recorded over each target. The first was recorded directly above the target and the remaining four were recorded at points offset from the point above the target to the north, south, east and west. This offset distance was about 6 inches for targets less than two feet deep, and about one foot for targets greater than two feet deep. The purpose of the off-set measurements was to demonstrate the insensitivity of the technique to uncertainty in the relative sensor/target position. After the five measurements were recorded, a single background measurement was made at a distance several feet away. This background measurement was subsequently subtracted from each of the

four target spectra to remove the response of the earth as well as the presence of any residual primary field due to imperfect bucking. Typically, the bucking will remove all but about one part in a thousand of the primary field at the receiver coil. For small, or deep, targets, this residual field can be a large fraction of the detected field.

As noted above, in computing the mean-square error using Eq. (12), it was found that matching the quadrature component only resulted in the fewest identification errors. This is because the inphase component was found to be considerably more sensitive than the quadrature to spatial and temporal variations in the background.

The five columns in Table 2 correspond to the five separate measurements for each target. The numbers in the table are mean-square error (MSE) ranks. In other words, a number 1 in the table indicates that the actual buried target listed in the left-hand column resulted in the smallest mean-square error, i.e., the target was correctly identified. The number 2 indicates that the true target produced the second smallest mean-square error, and so on. When different measurements over a given target give different MSE ranks, we employed a simple majority decision rule to select

Table 2. Mean-Square Error Ranks for the 21 Targets Buried at the Geophex Test Site. A Rank of "1" Means That the Target Was Correctly Identified

ID	1	2	3	4	5	Majority Rule	Sum
A ₁	1	4	2	1	1	1	1
A ₂	2	1	1	1	1	1	1
B ₁	1	1	1	1	1	1	1
B ₂	1	1	1	1	1	1	1
B ₃	4	4	2	4	4	4	4
C ₁	1	1	1	1	1	1	1
C ₂	1	2	1	2	1	1	1
C ₃	1	1	1	1	1	1	1
D	1	2	1	1	1	1	1
E ₁	1	1	1	1	1	1	1
E ₂	1	1	1	1	1	1	1
E ₃	1	2	1	2	2	2	1
E ₄	2	1	1	1	1	1	1
F ₁	2	2	3	3	3	3	3
F ₂	2	2	2	2	2	2	2
G ₁	1	1	1	1	1	1	1
G ₂	1	1	1	1	1	1	1
H ₁	1	1	1	1	1	1	1
H ₂	1	1	1	1	1	1	1
I ₁	1	1	1	1	1	1	1
I ₂	1	1	1	1	1	1	1

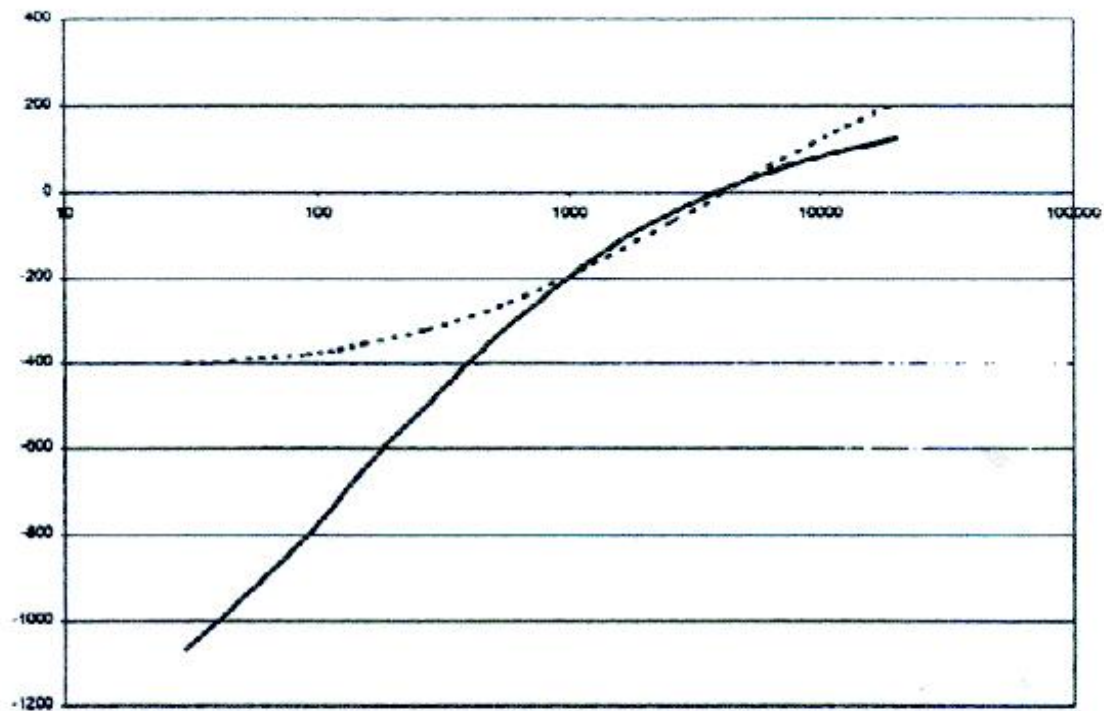
the most likely match. These are listed in the second to the last column in the table. Based on this rule, we see that, out of 21 targets, there were 17 correct identifications and 4 errors.

Another approach is to add together the five spectra before the fitting procedure is applied. This is a valid approach since the sum of a linear combination of $\beta_L(\omega)$ and $\beta_T(\omega)$ is again a linear combination. It might be expected that the sum of measurements recorded at different offsets could provide a somewhat more robust result since it combines measurements that view the target from different directions. The MSE rank computed using this method is listed in the last column in Table 2, labeled "sum." This procedure gives one less error than the "majority rule method," resulting in 18 correct identifications out of 21.

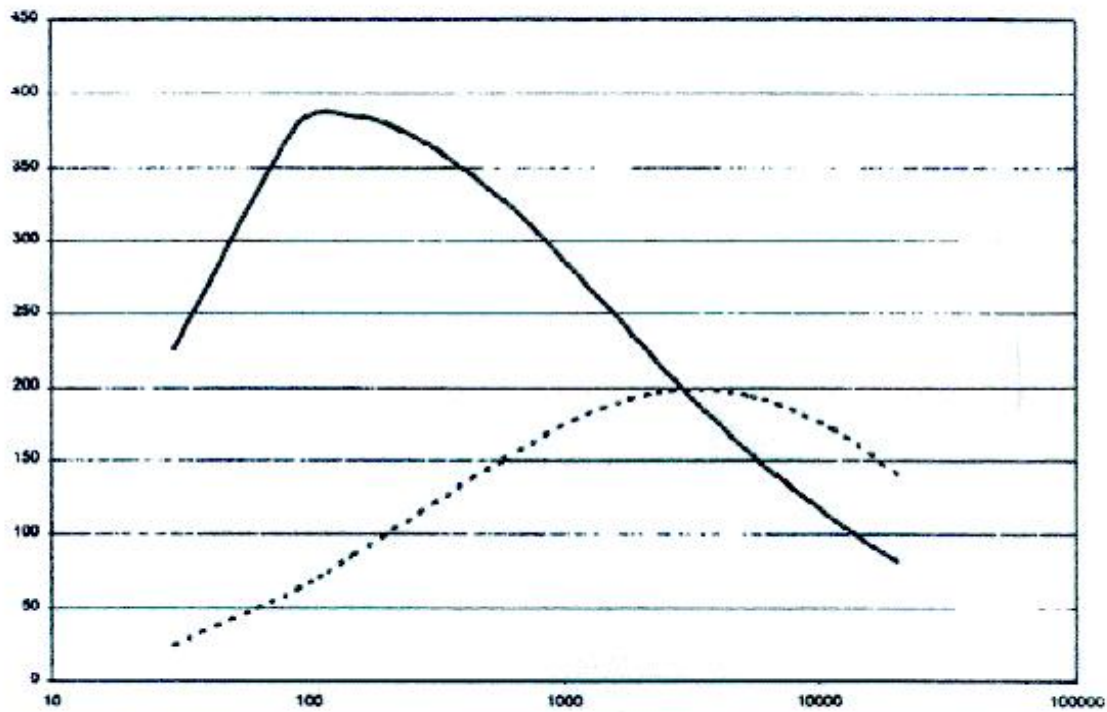
To illustrate how well the optimal linear combination of the longitudinal and transverse responses fit the data, we show in Figure 1 plots of $\beta_L(\omega)$ and $\beta_T(\omega)$ for target E₄. For this target, Figure 1a shows the inphase and quadrature components of the longitudinal response and Figure 1b shows the inphase and quadrature components of the transverse response $\beta_T(\omega)$. The data acquired from this buried target is plotted in Figure 2 (the solid curves) along with the fit to the data given by the optimal linear combination of $\beta_L(\omega)$ and $\beta_T(\omega)$ (the dashed curves). The plot shows, for this case, that a close fit is obtained.

4. Test Stand Data Using UXO

Data were also recorded from eleven different UXO, where each ordnance item was placed on a test stand below the sensor. The characteristics of the UXO are listed in Table 3. Sets of data were taken for each target in the vertical and horizontal orientations to obtain $\beta_L(\omega)$ and $\beta_T(\omega)$. A second set of measurements was taken at a 45 degree orientation at a greater sensor/target range (about 15 cm larger). The vertical and horizontal data were employed as our library spectra and the set of 45 degree measurements as our test spectra. The fitting procedure was again applied by computing the mean-square errors using Eq. (12). The MSE rank for the eleven UXO are listed in Table 4. Again, a rank of "1" indicates a correct identification and a rank greater than "1" indicates an incorrect identification. For example, the rank "4" for the 7.6 mm projectile indicates that this target produced the fourth smallest mean-square error. Table 4 shows that nine of the UXO items were correctly identified, with two errors. Improved results might be expected by increasing the number of frequencies beyond 10 and/or by expanding the bandwidth of the transmitted signal.

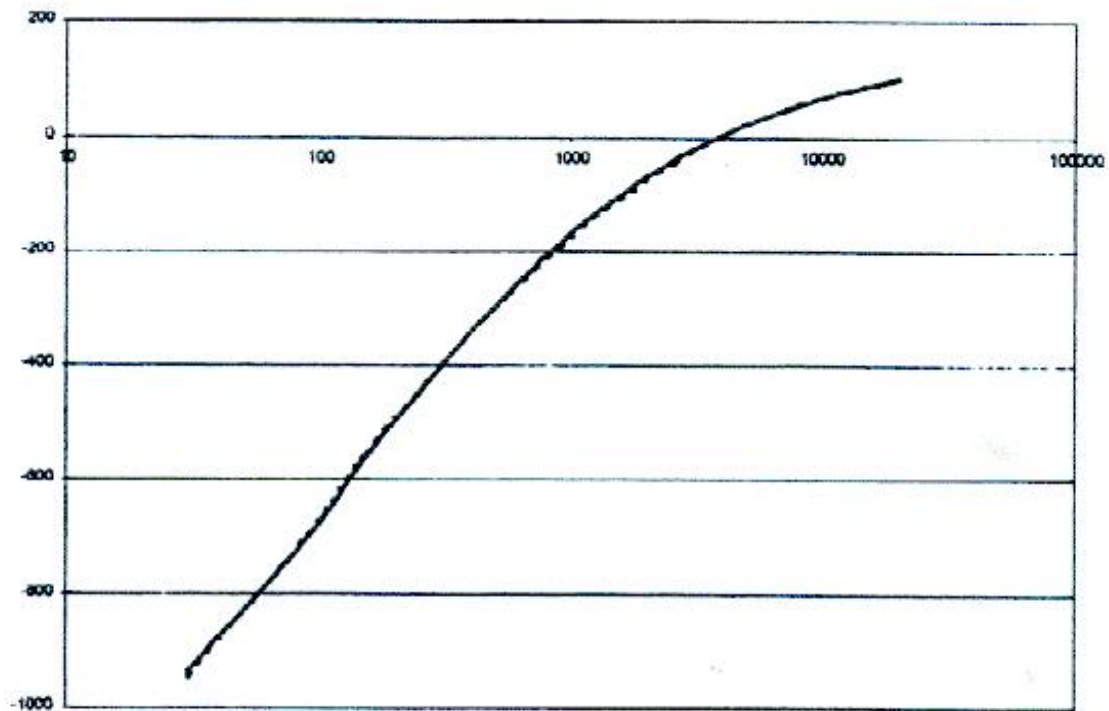


(a)

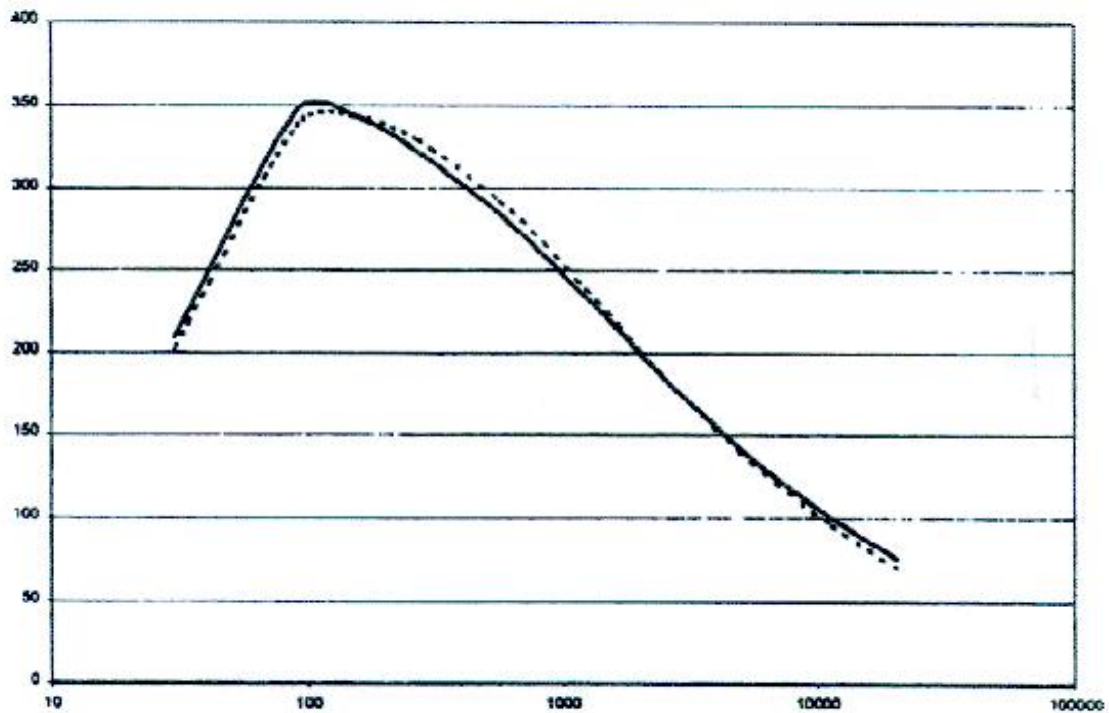


(b)

Figure 1. (a) The solid and dashed curves are respectively the inphase component of the longitudinal and transverse β_s ; (b) the solid and dashed curves are respectively the quadrature component of the longitudinal and transverse β_s . The horizontal axis is in Hz.



(a)



(b)

Figure 2. (a) The solid curve is the inphase component of the measured target spectrum and the dashed curve is the optimal linear combination of the inphase β s that provides the best fit to the measured response; (b) the quadrature spectrum and its best fit.

Table 3. UXO Tested

UXO	Type	Diameter	Length
20 mm	Projectile	2.0 cm	7.3 cm
60 mm	Mortar	6.0 cm	18.4 cm
60 mm	Mortar	6.0 cm	23.2 cm
57 mm	Projectile	5.7 cm	12.0 cm
105 mm	Projectile	10.5 cm	37.8 cm
4.2 inch	Mortar	10.7 cm	52.5 cm
76 mm	Projectile	7.6 cm	49.5 cm
81 mm	Mortar	8.1 cm	27.5 cm
152 mm	Projectile	15.2 cm	48.5 cm
2.75 inch	Rocket	7.0 cm	40.8 cm
5 inch	Projectile	12.7 cm	68.0 cm

5. Conclusion

We have developed and demonstrated a simple spectral matching procedure for identifying buried UXO by comparing their spectra to a set of pre-measured library spectra. The advantage of this approach is that it is insensitive to the target orientation and depth. Also, unlike dipole-fitting methods, accurate knowledge of the sensor position relative to the target is not needed. Our results suggest that the spectra of different UXO and sections of pipe are almost always sufficiently distinct to allow correct identification given an adequate target signal-to-noise ratio.

Acknowledgments

This work was funded by the US Army Corps of Engineers' Installation Restoration Research Program.

Table 4. UXO Identification Results

UXO Type	MSE Rank
20 mm	1
60 mm-a	1
60 mm-b	1
57 mm	1
105 mm	1
4.2 inch	1
7.6 mm	4
81 mm	1
152 mm	2
2.75 inch	1
5.0 inch	1

References

1. Won, I.J., Keiswetter, D.A., Fields, G.R.A., and Sutton, L. C., 1996, GEM-2: A new multifrequency electromagnetic sensor: *J. Env. Eng. Geophysics*, v. 1, p. 129–137.
2. Won, I.J., Keiswetter, D.A., Hanson, D.R., Novikova, E., and Hall, T.M., 1997, GEM-3: A monostatic broadband electromagnetic induction sensor: *J. Env. Eng. Geophysics*, v. 2, p. 53–64.
3. Won, I.J., Keiswetter, D.A., and Novikova, E., 1998, Electromagnetic induction spectroscopy: *J. Env. Eng. Geophysics*, v. 3, p. 27–40.
4. Bell, T.H., Barrow, B., and Khadr, N., 1998, Shape-based classification and discrimination of subsurface objects using electromagnetic induction: *Proceedings of the International Geoscience and Remote Sensing Symposium (IGARSS)*, Seattle, WA, July 6–10.
5. Bell, T.H., Barrow, B.J., and Miller, J.T., 2000, Subsurface discrimination using electromagnetic induction sensors: *SPIE Proceedings*, v. 4129, p. 120–129.
6. Ozdemir, M., Miller, E.L., and Norton, S.J., 1998, Localization and characterization of buried objects from multi-frequency, array inductive data: *SPIE Proceedings*, Orlando, FL.
7. Norton, S.J. and Won, I.J., 2001, Identification of buried unexploded ordnance from broadband electromagnetic induction data: *IEEE Trans. Geosci. Remote Sensing* (submitted).
8. Das, Y., McFee, J.E., Toews, J., and Stuart, G.C., 1990, Analysis of an electromagnetic induction detector for real-time location of buried objects: *IEEE Trans. Geosci. Remote Sensing*, GRS-28, p. 278–288.
9. Baum, C.E. (ed.), 1999, *Detection and identification of visually obscured targets*: Taylor and Francis, Philadelphia.
10. Burrows, M.L., 1964, A theory of eddy-current flaw detection, PhD Thesis, University of Michigan.